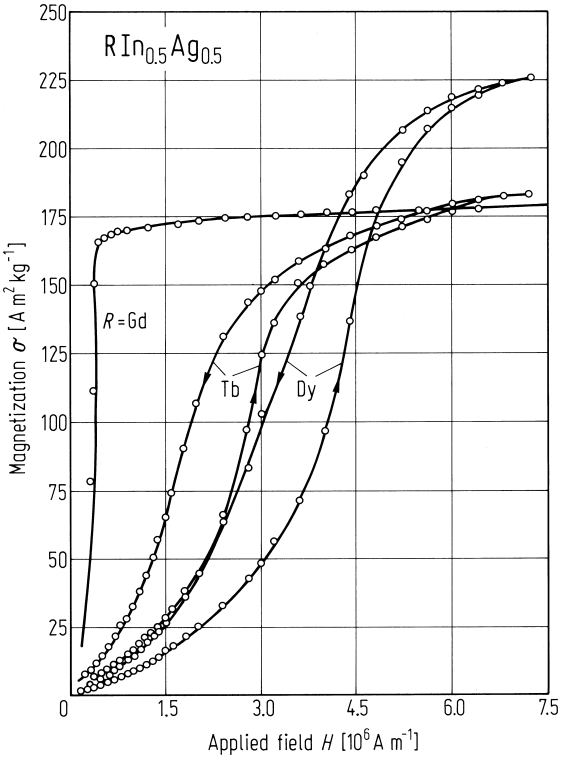

Fig. 179. Magnetisation vs. applied magnetic field for $RIn_{0.5}Ag_{0.5}$ with R = Gd, Tb, Dy [81L1].

1.5.5.3.3.5 Quaternary

The effects of electron concentration on the magnetic properties of Heusler alloys has been investigated in a series of quaternary compounds. Continuous Heusler series form at the intermediate compositions $Pd_2MnIn_{1-x}Sn_x$, $Pd_2MnSn_{1-y}Sb_y$ and $Pd_2MnIn_{1-x}Sb_x$ and the details have been summarised [88W1]. In these series three types of magnetic structure are observed, antiferromagnetic fcc type 2 (AF2), antiferromagnetic fcc type 3A (AF3A) and ferromagnetic. The results show a direct correlation between electron concentration and magnetic structure. Similar behaviour has been observed in the series $Pd_{2-x}Cu_xMnIn$ [88W1] in which substitution is made at the X site rather than the Z site.

$X_2(YY^*)Z$ X = 3d, Y= Y* = 3d

X = 8A: Fe
Y = 7A: Mn
Y* = 5A: V
Z = 4B: Sn

$Fe_2Mn_{1-x}V_xSi$

Single phase compounds with the $L2_1$ structure form for the entire composition range $0 \le x \le 1$. The Curie temperature increases from 219 K for x = 0 to 315 K at x = 0.5. For x > 0.5 the Curie temperature decreases rapidly, vanishing at x = 0.86.

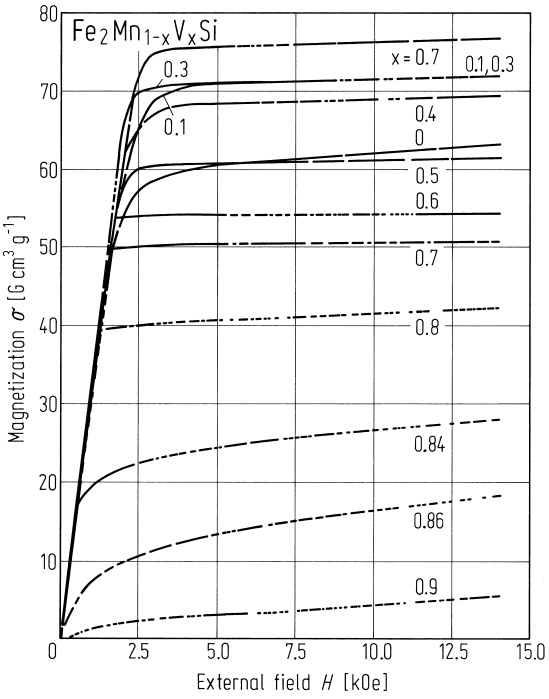

Fig. 180. Plots of the magnetisation σ at 4.2 K as a function of the external magnetic field H for various values of x in $Fe_2Mn_{1-x}V_xSi$ [93K1].

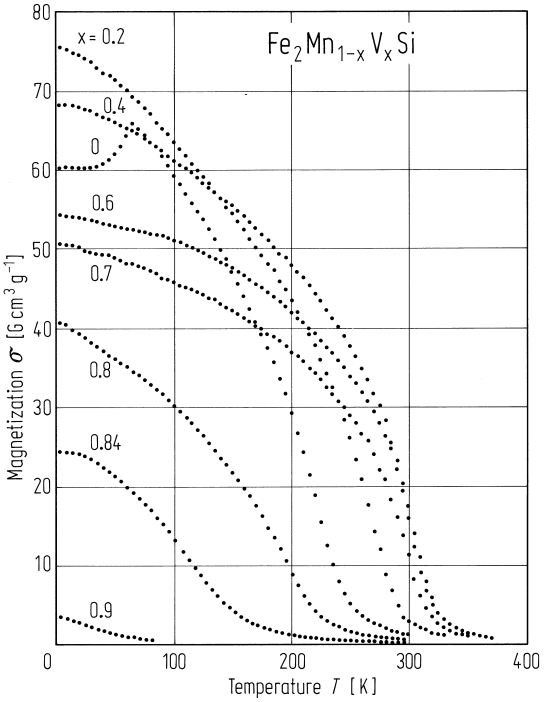

Fig. 181. Plots of the magnetisation σ at 4.7 kOe as a function of temperature T for various values of x in $Fe_2Mn_{1-x}V_xSi$ [93K1].

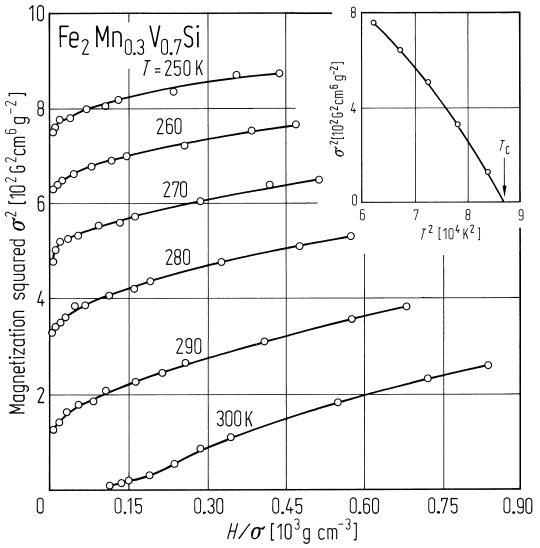

Fig. 182. Arrott plots of σ^2 vs. H/σ and plots of σ^2 against T^2 (inset) for $Fe_2Mn_{0.3}V_{0.7}Si$ [93K1].

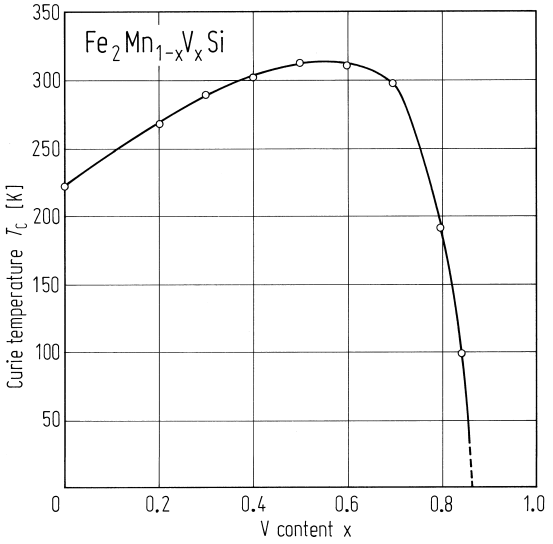

Fig. 183. Curie temperature T_C as a function of V concentration x in $Fe_2Mn_{1-x}V_xSi$ [93K1].

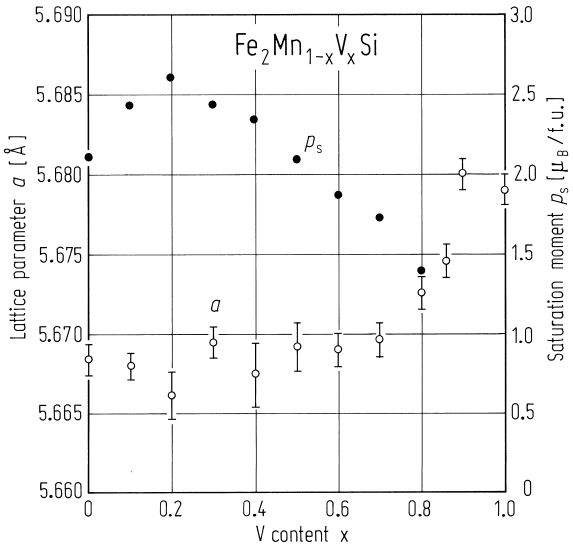

Fig. 184. Lattice parameter a and saturation moments p_s per formula unit in $Fe_2Mn_{1-x}V_xSi$ [93K1].

(XX*)YZ X, X* = 3d, Y = 3d

X = 8A: Co
X*= 8A: Fe
Y = 7A: Mn
Z = 4B: Si

$Co_{2-x}Fe_xMnSi$

Single phase compounds with the $L2_1$ structure form for the entire composition range $0 \le x \le 2$. The Curie temperature decreases continuously with increasing x.

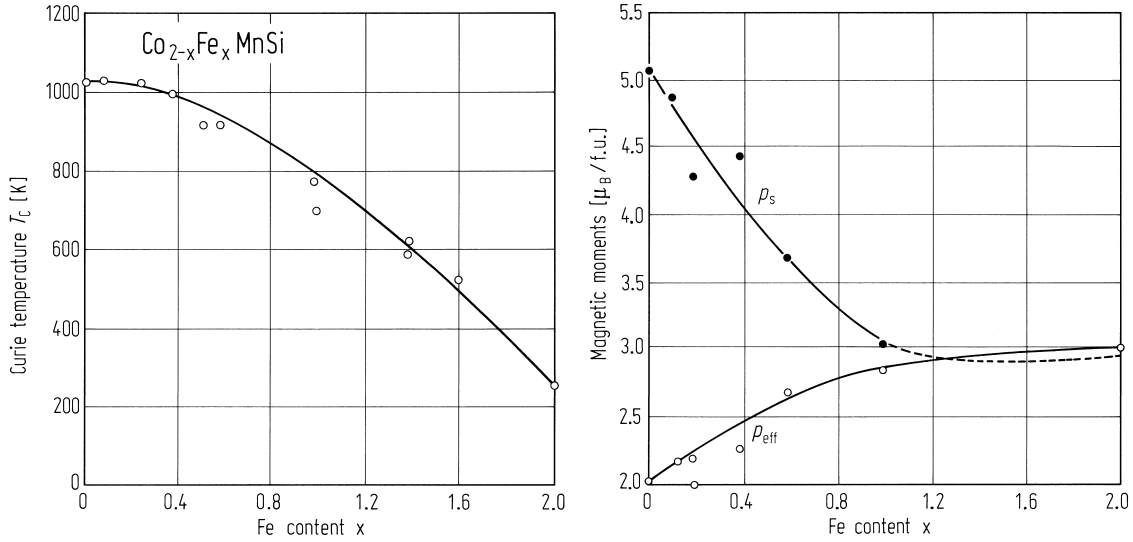

Fig. 185. Variation of the Curie temperature T_C, the ferromagnetic moment per f.u., p_s and the effective paramagnetic moment p_{eff} in $Co_{2-x}Fe_xMnSi$ [88I1].

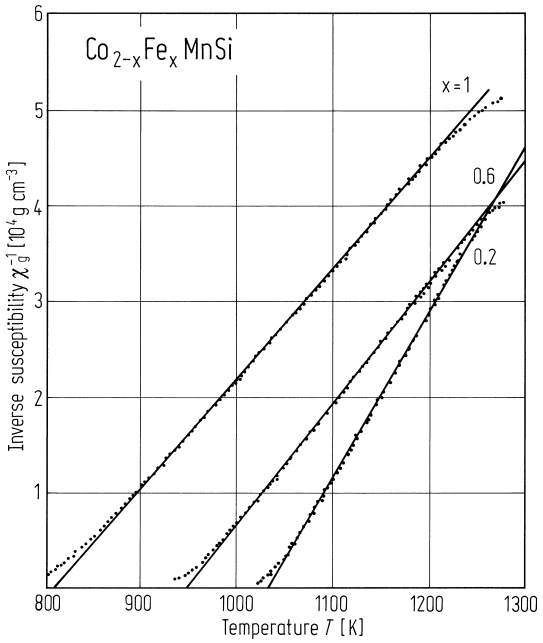

Fig. 186. Reciprocal susceptibility vs. temperature for Fe modified Co_2MnSi. For x = 0.2: p = 2.20 μ_B, Θ = 1031.5 K, T_C = 1025.3 K; x = 0.6: p = 2.67 μ_B, Θ = 945 K, T_C = 920 K; x = 1: p = 2.85 μ_B, Θ = 805 K, T_C = 777 K [86I1].

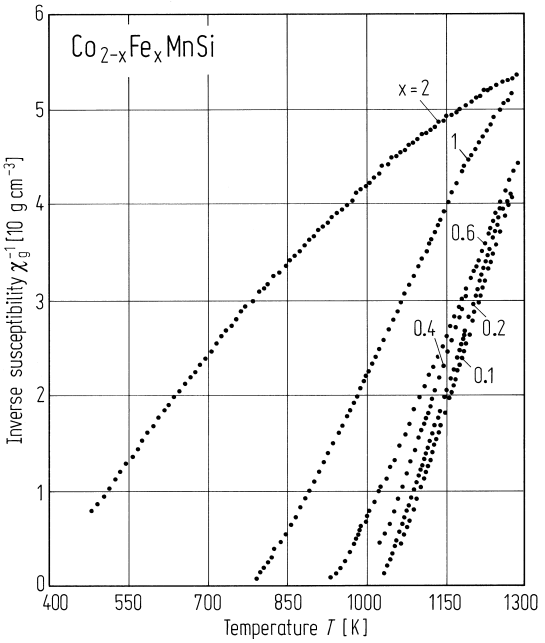

Fig. 187. Reciprocal susceptibility vs. temperature curves for $Co_{2-x}Fe_xMnSi$ [88I1].

(XX*)YZ X, X* = 3d, Y = 3d

X = 8A: Co
X* = 8A: Fe; 1B: Cu
Y = 7A: Mn
Z = 4B: Ge

$Co_{2-x}Fe_xMnGe$

Single phase compounds with the $L2_1$ structure only form for compositions x ≤ 1.2.

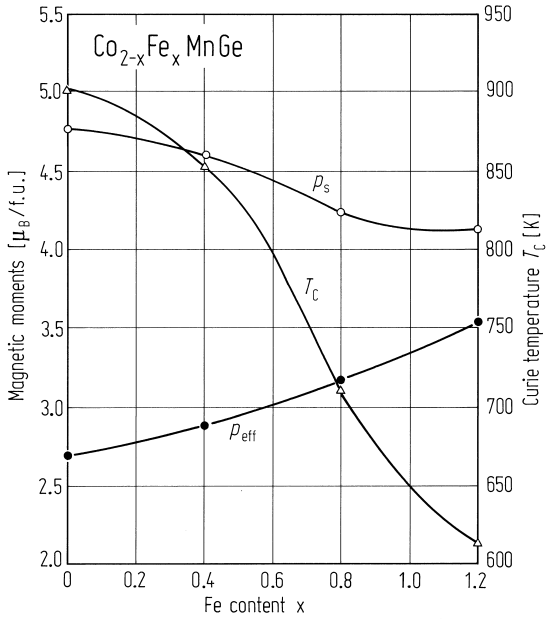

Fig. 188. Magnetic moment p_s obtained from saturation magnetisation at 77 K and p_{eff} from χ^{-1} vs. T curves above T_C for Fe-modified Co_2MnGe [86I1].

$Co_{2-x}Cu_xMnSn$

Single phase compounds with the $L2_1$ structure form for the entire composition range $0 \le x \le 2$. The Curie temperature decreases with x up to 1.4 and then increases with further copper content.

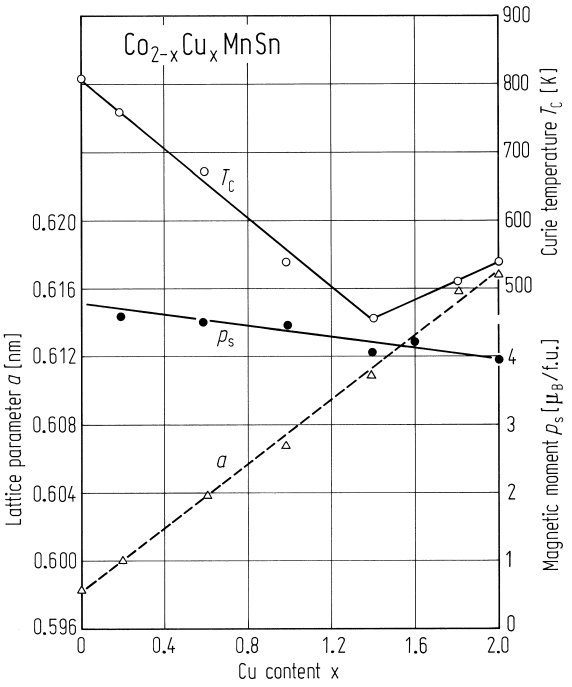

Fig. 189. Lattice constant a, saturation moment p_s at 4.2 K, and Curie temperature T_C as a function of concentration x in Heusler alloys of the type $Co_{2-x}Cu_xMnSn$ [87V1].

(XX*)YZ X, X* = 3d, Y = 3d

X = 8A: Co
X* = 8A: Ni
Y = 4A: Ti
Z = 4B: Sn

$Co_xNi_{1-x}TiSn$

Compounds in the series $0 \le x \le 1$ order in the $C1_b$ or $L2_1$ structures. Both the effective and ferromagnetic moments, together with Curie temperature, increase with the cobalt content.

Table 35. Magnetic properties of some cobalt-based Heusler alloys [94P2].

Compound	Θ [K]	p_{eff} [μ_B]	p_s [μ_B]	T_C [K]	$p_{eff}/p(0)$
$TiCo_2Sn$	370	1.96	0.98	370	1.98
TiCoSn	158	1.35	0.357	134	3.78
$TiCo_{1.4}Ni_{0.6}Sn$	115	1.42	0.166	53	8.6
$TiCo_{0.5}Ni_{0.5}Sn$	7.5	1.32	0.074	5	18

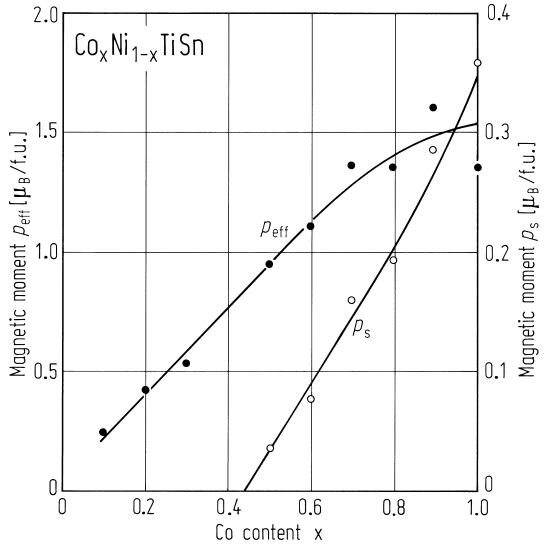

Fig. 190. Effective paramagnetic moment and saturation magnetisation (per formula unit) in $Co_xNi_{1-x}TiSn$ vs. Co content [94P1].

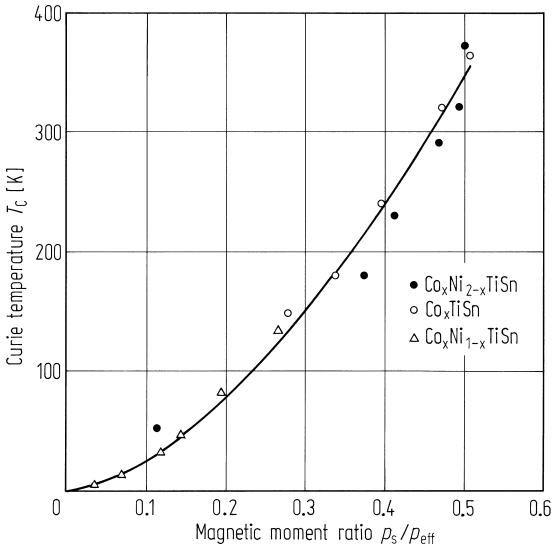

Fig. 191. Ferromagnetic Curie temperature vs. the ratio p_s/p_{eff} in $Co_xNi_{2-x}TiSn$, Co_xTiSn and $Co_xNi_{1-x}TiSn$ [94P1].

(XX*)YZ **X = 3d, X* = 4d, Y = 3d**

X = 8A: Co, Ni
X* = 8A: Rh, Pd
Y = 7A: Mn
Z = 4B: Sn

$(Pd_{1-x}Co_x)_2MnSn$

Single phase compounds with the $L2_1$ structure form for $0 \leq x \leq 1$. All the compounds order ferromagnetically with Curie temperatures between 190 K and 830 K.

Table 36. Ferromagnetic saturation moment p_s, Curie temperature T_C, paramagnetic Curie temperature Θ, paramagnetic moment p_{eff} and lattice parameter a of $(Pd_{1-x}Co_x)_2MnSn$ [85U1].

Alloy	p_s (exp) [μ_B]	$p_{s\,Mn}$ (calc) [μ_B]	p_s (calc) [μ_B]	T_C [K]	Θ [K]	p_{eff} (exp) [μ_B]	p_{eff} (calc) [μ_B]	a [Å]
Pd_2MnSn	4.21	4.20	4.20	188	202	5.01	4.90	6.380
$Pd_{1.9}Co_{0.1}MnSn$	4.34	4.17	4.27	220	235	5.03	4.93	6.362
$Pd_{1.8}Co_{0.2}MnSn$	4.41	4.14	4.34	250	265	4.97	4.96	6.343
$Pd_{1.6}Co_{0.4}MnSn$	4.43	4.08	4.48	310	331	5.03	5.02	6.307
$Pd_{1.4}Co_{0.6}MnSn$	4.68	4.02	4.62	375	400	5.10	5.08	6.269
$Pd_{1.2}Co_{0.8}MnSn$	4.83	3.96	4.76	440	461	5.16	5.14	6.232
$Pd_{1.0}Co_{1.0}MnSn$	4.97	3.90	4.90	511	537	5.11	5.20	6.192
$Pd_{0.8}Co_{1.2}MnSn$	5.12	3.84	5.04	565	594	5.19	5.25	6.156
$Pd_{0.6}Co_{1.4}MnSn$	5.24	3.78	5.18	628	661	5.22	5.31	6.116
$Pd_{0.4}Co_{1.6}MnSn$	5.25	3.72	5.32	704	728	5.20	5.37	6.071
$Pd_{0.2}Co_{1.8}MnSn$	5.33	3.66	5.46	766	802	5.26	5.42	6.037
$Pd_{0.1}Co_{1.9}MnSn$	5.42	3.63	5.53	795	828	5.37	5.45	6.020
Co_2MnSn	5.02	3.60	5.10	825	856	5.29	5.30	5.999

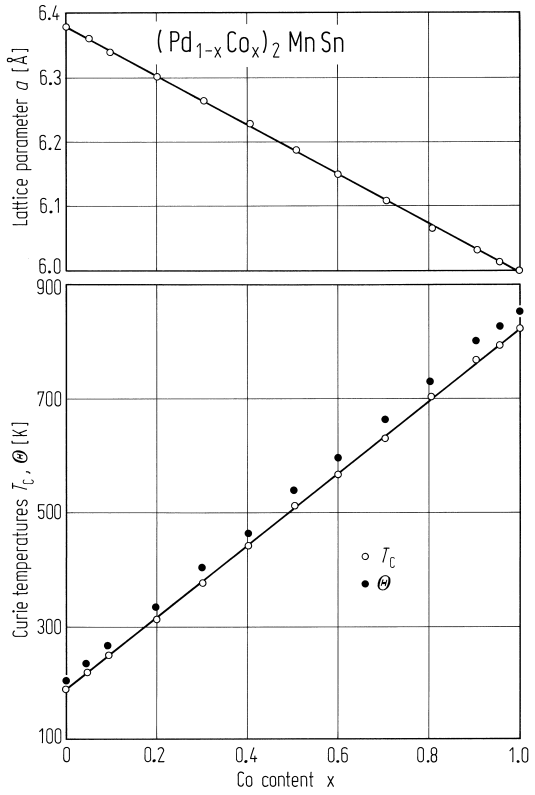

Fig. 192. Lattice parameter a, Curie temperature T_C and paramagnetic Curie temperature Θ of the alloy series $(Pd_{1-x}Co_x)_2MnSn$. The straight line connects the lattice parameters of the ternaries [85U1].

$(Pd_{1-x}Ni_x)_2MnSn$

Single phase compounds with the $L2_1$ structure form between Pd_2MnSn and Ni_2MnSn. All the compounds are ferromagnetic with Curie temperatures between 190…340 K.

Table 37. Ferromagnetic saturation moment p_s, Curie temperature T_C, paramagnetic Curie temperature Θ, paramagnetic moment p_{eff}, ratio of magnetic carriers in the para and ferromagnetic state, p_P/p_s, and lattice parameter a of $(Pd_{1-x}Ni_x)_2MnSn$ [85U1].

Alloy	p_s [μ_B]	T_C [K]	Θ [K]	p_{eff} [μ_B]	p_P/p_s	a [Å]
Pd_2MnSn	4.21	188	202	5.01	0.98	6.380
$Pd_{1.9}Ni_{0.1}MnSn$	4.15	196	211	5.00	0.99	6.367
$Pd_{1.8}Ni_{0.2}MnSn$	4.12	202	218	4.98	0.99	6.345
$Pd_{1.6}Ni_{0.4}MnSn$	4.10	213	231	4.98	0.99	6.312
$Pd_{1.4}Ni_{0.6}MnSn$	4.07	229	245	4.95	1.00	6.284
$Pd_{1.2}Ni_{0.8}MnSn$	4.02	248	260	4.86	0.99	6.250
$Pd_{1.0}Ni_{1.0}MnSn$	4.10	259	280	4.93	0.98	6.220
$Pd_{0.8}Ni_{1.2}MnSn$	4.04	281	300	4.83	0.97	6.186
$Pd_{0.6}Ni_{1.4}MnSn$	4.07	290	314	4.89	0.98	6.153
$Pd_{0.4}Ni_{1.6}MnSn$	4.04	309	335	4.88	0.99	6.120
$Pd_{0.2}Ni_{1.8}MnSn$	3.92	320	350	4.93	1.03	6.089
$Pd_{0.1}Ni_{1.9}MnSn$	3.94	328	352	4.87	1.00	6.066
Ni_2MnSn	3.98	342	363	4.90	1.00	6.052

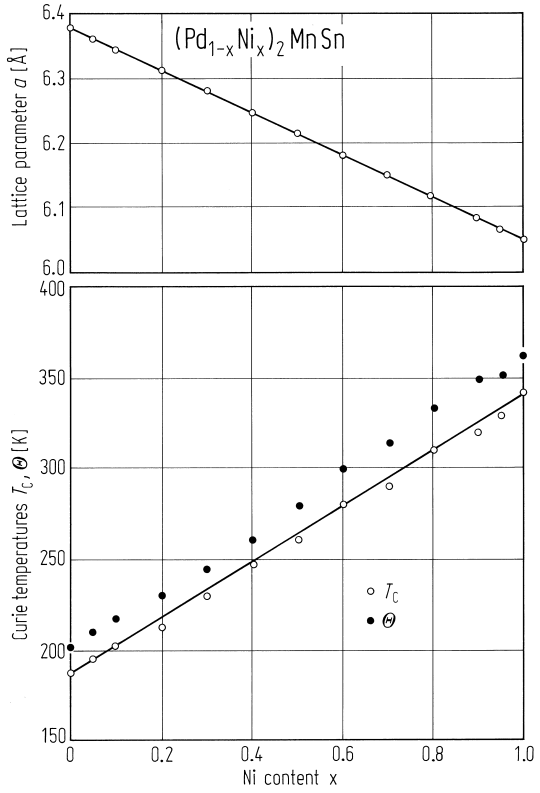

Fig. 193. Lattice parameter *a*, Curie temperature T_C and paramagnetic Curie temperature Θ of the alloy series $(Pd_{1-x}Ni_x)_2MnSn$. The straight line connects the lattice parameters of the ternaries [85U1].

$(Rh_{1-x}Ni_x)_2MnSn$

Single phase compounds with the $L2_1$ structure form for all compositions between Rh_2MnSn and Ni_2MnSn. All the materials are ferromagnetic with a moment on the Mn atoms of $\approx 4\ \mu_B$.

Table 38. Ferromagnetic saturation moment p_s, Curie temperature T_C, paramagnetic Curie temperature Θ, paramagnetic moment p_{eff}, ratio of magnetic carrieres in the para-and ferromagnetic state, p_P/p_s, and lattice parameter *a* of $(Rh_{1-x}Ni)_2MnSn$ [85U2].

Alloy	p_s [μ_B]	T_C [K]	Θ [K]	p_{eff} [μ_B]	p_P/p_s	*a* [Å]
Rh_2MnSn	4.14	410	412	4.83	0.95	6.252
$Rh_{1.9}Ni_{0.1}MnSn$	4.03	392	401	4.86	0.98	6.245
$Rh_{1.8}Ni_{0.2}MnSn$	4.00	382	392	4.94	1.01	6.233
$Rh_{1.6}Ni_{0.4}MnSn$	4.06	364	380	4.91	0.99	6.209
$Rh_{1.4}Ni_{0.6}MnSn$	4.05	346	364	4.88	0.98	6.187
$Rh_{1.2}Ni_{0.8}MnSn$	4.05	337	352	4.87	0.98	6.170
$Rh_{1.0}Ni_{1.0}MnSn$	4.04	327	345	4.90	0.99	6.149
$Rh_{0.8}Ni_{1.2}MnSn$	4.05	324	340	4.89	0.99	6.132
$Rh_{0.6}Ni_{1.4}MnSn$	4.03	321	336	4.94	1.00	6.117
$Rh_{0.4}Ni_{1.6}MnSn$	4.02	325	340	4.91	1.00	6.095
$Rh_{0.2}Ni_{1.8}MnSn$	4.13	331	348	4.93	0.98	6.075
$Rh_{0.1}Ni_{1.9}MnSn$	4.07	335	355	4.91	0.99	6.068
Ni_2MnSn	3.98	342	363	4.90	1.00	6.052

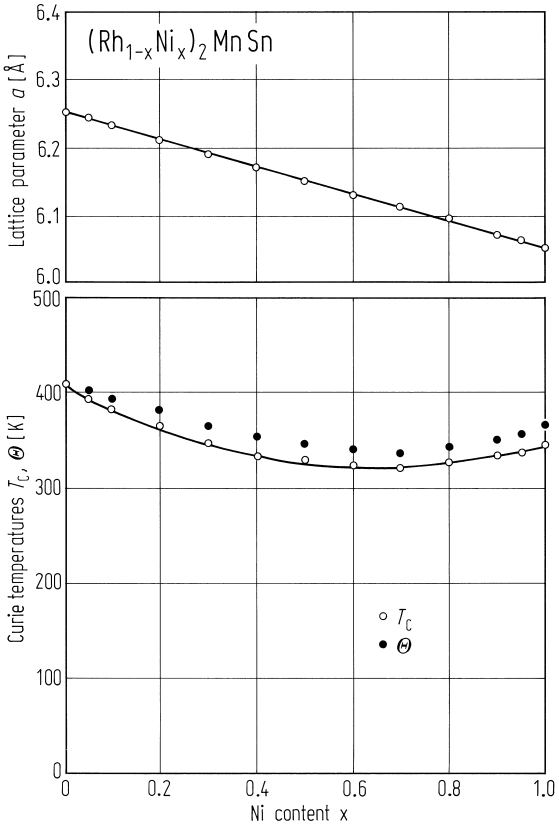

Fig. 194. Lattice parameter *a*, Curie temperature T_C and paramagnetic Curie temperature Θ of the alloy series $(Rh_{1-x}Ni_x)_2MnSn$. The straight line connects the lattice parameters of the ternaries [85U2].

$(Rh_{1-x}Co_x)_2MnSn$

All the compounds between Rh_2MnSn and Co_2MnSn have the Heusler structure. Depending on the Co content, the moment on the Mn atoms is between 3.6…4 μ_B.

Table 39. Ferromagnetic saturation moment p_s, Curie temperature T_C, paramagnetic Curie temperature Θ, paramagnetic moment p_{eff} and lattice parameter *a* of $(Rh_{1-x}Co_x)_2MnSn$ [85U2].

Alloy	p_s (exp) [μ_B]	$p_{s\,Mn}$ (calc) [μ_B]	p_s (calc) [μ_B]	T_C [K]	Θ [K]	p_{eff} (exp) [μ_B]	p_{eff} (calc) [μ_B]	*a* [Å]
Rh_2MnSn	4.14	4.10	4.10	410	412	4.83	4.90	6.252
$Rh_{1.9}Co_{0.1}MnSn$	4.20	4.08	4.16	455	457	4.90	4.92	6.236
$Rh_{1.8}Co_{0.2}MnSn$	4.31	4.05	4.20	492	507	4.79	4.94	6.225
$Rh_{1.6}Co_{0.4}MnSn$	4.49	4.00	4.30	590	606	4.92	4.98	6.204
$Rh_{1.4}Co_{0.6}MnSn$	4.50	3.95	4.40	635	651	5.06	5.02	6.176
$Rh_{1.2}Co_{0.8}MnSn$	4.59	3.90	4.50	666	691	5.09	5.06	6.148
$Rh_{1.0}Co_{1.0}MnSn$	4.72	3.85	4.60	687	715	5.12	5.10	6.130
$Rh_{0.8}Co_{1.2}MnSn$	4.79	3.80	4.70	720	738	4.98	5.14	6.106
$Rh_{0.6}Co_{1.4}MnSn$	4.85	3.75	4.80	749	767	5.03	5.18	6.074
$Rh_{0.4}Co_{1.6}MnSn$	4.94	3.70	4.90	770	792	5.06	5.22	6.047
$Rh_{0.2}Co_{1.8}MnSn$	5.00	3.65	5.00	800	827	5.27	5.26	6.028
$Rh_{0.1}Co_{1.9}MnSn$	5.02	3.63	5.06	811	838	5.24	5.28	6.013
Co_2MnSn	5.02	3.60	5.10	825	856	5.29	5.30	5.999

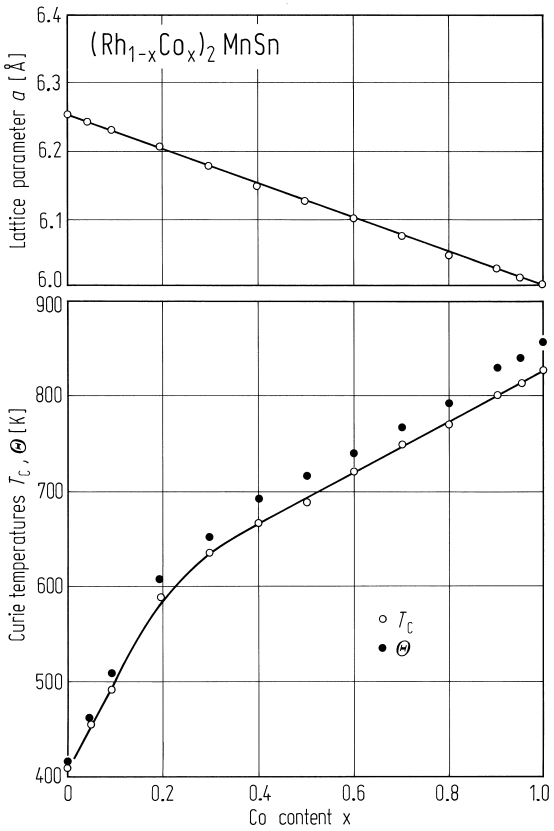

Fig. 195. Lattice parameter a, Curie temperature T_C and paramagnetic Curie temperature Θ) of the alloy series $(Rh_{1-x}Co_x)_2MnSn$. The straight line connects the lattice parameters of the ternaries [85U2].

(XX*)YZ X, X* = 4d, Y = 3d

X = 8A: Pd
X* = 1B: Ag
Y = 7A: Mn
Z = 3B: In

$Pd_{2-x}Ag_xMnIn$

Single phase compounds with the $L2_1$ structure only form for compositions with $x < 0.8$. (See Fig. 196.)

(XX*)YZ X = 4d, X* = 5d, Y = 3d

X = 8A: Pd
X* = 1B: Au
Y = 7A: Mn
Z = 3B: In

$Au_xPd_{2-x}MnIn$

Single phase compounds with the $L2_1$ structure form for all values of x with $0 \le x \le 1$. In all previous quaternary systems based on Pd_2MnIn the only antiferromagnetic structures observed have been the AF2 and AF3A. However, in the middle of the $Au_xPd_{2-x}MnIn$ series an additional magnetic structure has been observed. This phase has been identified as fcc antiferromagnetism type 1 (AF1) which has a propagation vector along the [001] direction [92J1]. A tetragonal lattice distortion accompanies the onset of antiferromagnetic order. The magnetic phase diagram is shown in Fig. 197.

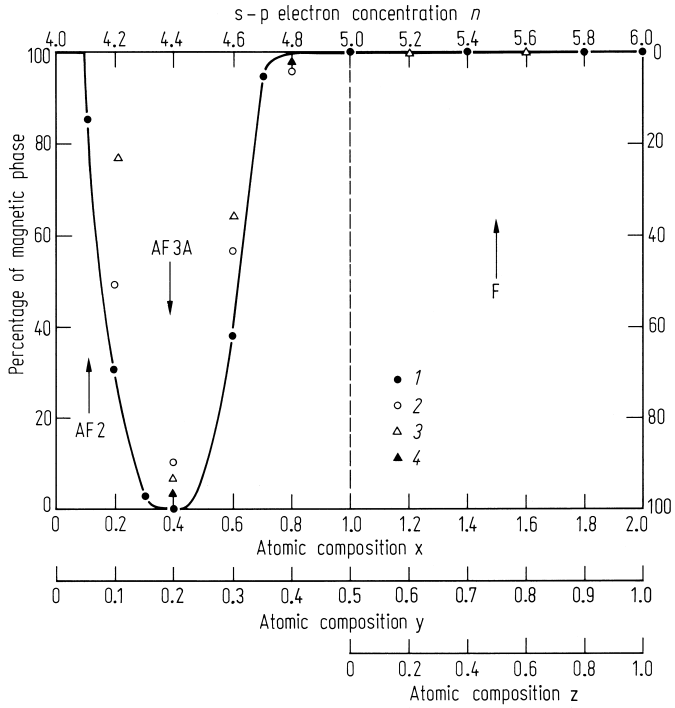

Fig. 196. Proportions of fcc antiferromagnetic phases AF2, AF3A and ferromagnetic vs. atomic compositions x, y and z and electron concentrations *n* for the series *1*: $Pd_2MnIn_{1-x}Sn_x$, $Pd_2MnSn_{1-z}Sb_z$; *2*: $Pd_2MnIn_{1-y}Sb_y$; *3*: $Pd_{2-x}Cu_xMnIn$; *4*: $Pd_{2-x}Ag_xMnIn$ [86W1].

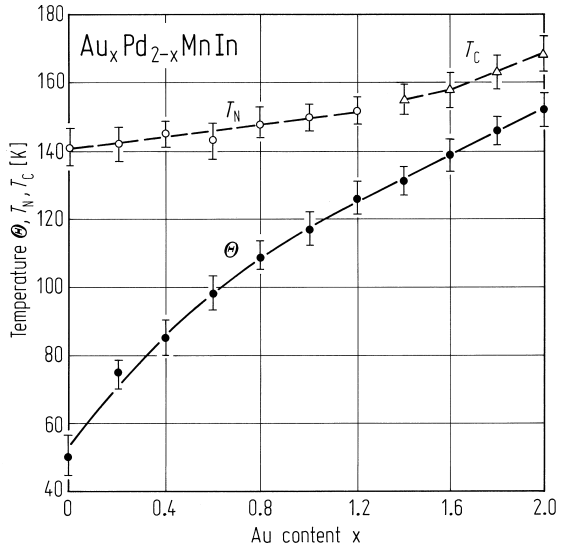

Fig. 197. Variation of the Néel (T_N), Curie (T_C) and paramagnetic Curie (Θ) temperature vs. composition x in $Au_xPd_{2-x}MnIn$ [90J1].

Table 40. A summary of the magnetic properties of $Pd_{2-x}Au_xMnIn$ compounds [90J1].

Alloy	a_o [Å]	Θ [K]	T_C or T_N [K]	p_{eff} [μ_B]	S	Phase transition from C_p	Magnetic structure	p [μ_B]	n_e
$Pd_{1.8}Au_{0.2}MnIn$	6.341 ± 0.003	75 ± 3	142 ± 3	4.50 ± 0.02	1.804	145 ± 2	AF2, AF3	5.40 ± 0.2	4.2
$Pd_{1.6}Au_{0.4}MnIn$	6.349 ± 0.003	85 ± 2	145 ± 3	4.60 ± 0.02	1.853	143 ± 3	AF3, AF2	3.921 ± 0.2	4.4
$Pd_{1.4}Au_{0.6}MnIn$	6.413 ± 0.003	98 ± 2	143 ± 3	4.52 ± 0.02	1.816	146 ± 2	AF1, AF3	4.98 ± 0.2	4.6
$Pd_{1.2}Au_{0.8}MnIn$	6.448 ± 0.003	109 ± 3	148 ± 2	4.75 ± 0.03	1.928	150 ± 2	AF1, AF3	4.11 ± 0.2	4.8
PdAuMnIn	6.463 ± 0.003	117 ± 3	150 ± 3	4.67 ± 0.02	1.889	151 ± 3	AF1, AF3	4.32 ± 0.2	5.0
$Pd_{0.8}Au_{1.2}MnIn$	6.522 ± 0.003	126 ± 3	152 ± 2	4.68 ± 0.03	1.895	153 ± 2	AF1, AF3,	3.91 ± 0.2	5.2
$Pd_{0.6}Au_{1.4}MnIn$	6.544 ± 0.003	131 ± 3	155 ± 2	4.78 ± 0.02	1.943	159 ± 3	AF1, AF3, F	4.73 ± 0.2	5.4
$Pd_{0.4}Au_{1.6}MnIn$	6.566 ± 0.003	139 ± 3	158 ± 2	4.85 ± 0.02	1.977	163 ± 3	F	4.1 ± 0.2	5.6
$Pd_{0.2}Au_{1.8}MnIn$	6.599 ± 0.003	146 ± 2	146 ± 2	4.99 ± 0.03	2.047	161 ± 3	F	4.12 ± 0.2	5.8
Au_2MnIn	6.644 ± 0.003	152 ± 2	168 ± 2	5.04 ± 0.03	2.070	164 ± 2	F		6.0

$X_2(YY^*)Z$ X = 3d, Y =4d, Y* = 4f

X = 8A: Pd
Y = 3A: Y
Y* = 4A: Dy
Z = 4B: Sn

$Pd_2Y_{1-x}Dy_xSn$

Heusler alloys with the $L2_1$ structure form at all compositions $0 \leq x \leq 1$. Depending upon composition the compounds are superconducting or antiferromagnetic.

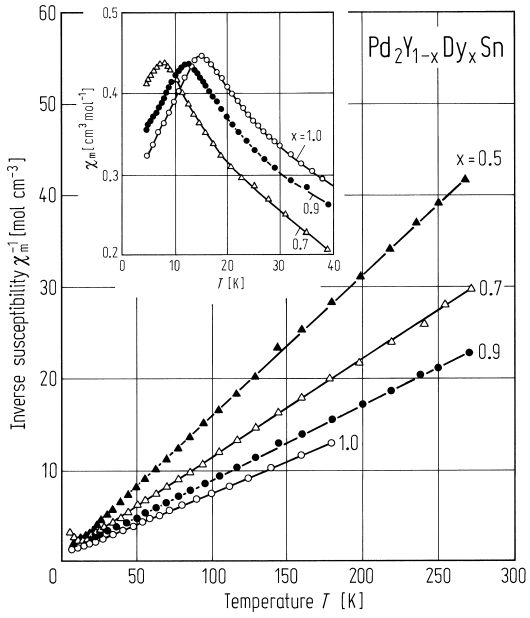

Fig. 198. Susceptibility and reciprocal susceptibility vs. temperature for several $Pd_2(Y_{1-x}Dy_x)Sn$ alloys [86M2].

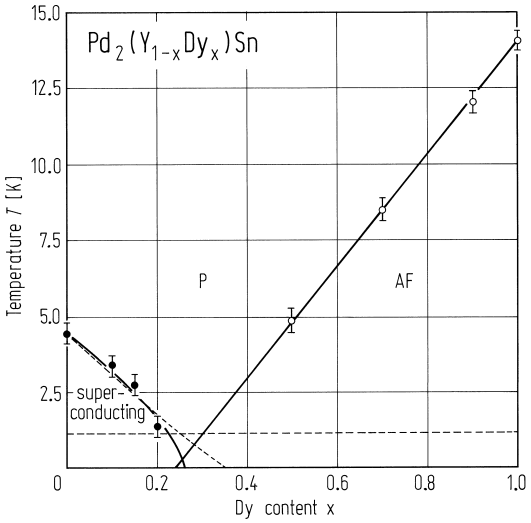

Fig. 199. Magnetic phase diagram of $Pd_2(Y_{1-x}Dy_x)Sn$. The dashed line represents the lowest temperature at which χ_{ac} measurements were made [86M2].

1.5.5.4 Neutron scattering

Details of the neutron scattering technique and the information which can be obtained were discussed in the earlier review [88W1].

1.5.5.4.1 Neutron diffraction

Neutron diffraction enables both the crystallographic and magnetic structures to be determined. To date the majority of investigations have been carried out on powders, using a profile refinement technique. The weak interaction of neutrons with matter, and the fact that the scattering amplitudes do not vary sequentially from element to element means that they are more attractive than X-rays for structural investigations. This is particularly the case if the temperature or pressure is to be changed. Whilst there are an infinite number of ways in which the atoms X_2YZ may arrange themselves in the $L2_1$ structure (see subsect. 1.5.5.2.1) it is normally possible to identify one of the preferential states of atomic order. The most prevalent type of atomic disorder occurring in Heusler alloys is the B2-